Numerical study of miscible fingering in a time-dependent gap Hele-Shaw cell

Ching-Yao Chen,[1,*] Chen-Hau Chen,[1,2] and José A. Miranda[3,†]
[1]*Department of Mechanical Engineering, National Yunlin University of Science & Technology, Yunlin, Taiwan, Republic of China*
[2]*Department of Automation Engineering, Nan-Kai Institute of Technology, Nantou, Taiwan, Republic of China*
[3]*Laboratório de Física Teórica e Computacional, Departamento de Física, Universidade Federal de Pernambuco, Recife, Pernambuco 50670-901 Brazil*

(Received 5 November 2004; revised manuscript received 18 January 2005; published 20 May 2005)

We perform a detailed numerical study of the evolution of a miscible fluid droplet in a time-dependent gap Hele-Shaw cell. The development of the emerging fingering instabilities is systematically analyzed by intensive and highly accurate numerical simulations. We focus on the influence of three relevant physical parameters on the interface dynamics: the Péclet number Pe, the viscosity contrast A, and the Korteweg stress parameter δ. Consistently with conventional miscible Saffman-Taylor studies in constant-gap Hele-Shaw cells, our results demonstrate that more vigorous fingering is observed at higher Pe and larger A. Concerning the specific role of Pe and A, we deduce two general results: higher Péclet number favors branching around a nearly circular region (which leads to longer interfacial lengths); while larger viscosity contrast results in more significant finger penetrations (which is quantitatively expressed by larger diameter of gyration). We have also verified that the Korteweg stress parameter δ does act as an effective interfacial tension: it stabilizes the miscible interface, leading to fingering patterns that present a greater resemblance with the structures obtained in similar immiscible situations. Finally, we have identified the development of a visually striking phenomenon in the limit of high Pe, large A, and relatively small δ: some outward fingers pinch, and subsequent droplet detachment is observed. We show that such a droplet detachment process can be prevented by the action of stronger interfacial stresses. This last finding provides additional evidence for the claim that the Korteweg stresses can be treated as an ersatz interfacial tension in diffusing fluids.

DOI: 10.1103/PhysRevE.71.056304 PACS number(s): 47.54.+r, 47.20.Ma, 47.11.+j, 64.75.+g

I. INTRODUCTION

Viscous fingering is one celebrated example of pattern forming systems where the nonlinear development of an instability can be studied in considerable detail. For this reason the Saffman-Taylor instability [1] has attracted a lot of interest during the last few decades [2]. It arises when a less viscous fluid pushes a more viscous one in the narrow gap separating two flat, parallel glass plates (Hele-Shaw cell). As a result of such hydrodynamic instability, a variety of patterned structures may develop at the fluid-fluid interface. If the flow occurs in rectilinear channels (rectangular geometry) the less viscous fluid takes the shape of a long, smooth bubble or "finger" [1]. On the other hand, branched and much more intricate interfacial patterns are formed if the less viscous fluid is injected through a hole located on the upper plate, and flows radially (radial geometry) [3]. Many theoretical and experimental studies have been performed in both geometries, leading to a good understanding of the basic physical mechanisms related to finger shape selection in rectangular geometry, and to tip-splitting events in the radial case.

Much of the research in this area has examined the flow in flat, motionless, constant-gap spacing Hele-Shaw cells, in which the fluids involved are relatively simple, usually immiscible and Newtonian. However, the quest for new morphologies and richer dynamic behavior resulted in a number of modifications of the classic Saffman-Taylor setup. Researchers have introduced changes into the system in many different ways: (i) by modifying the shape of the cell, and considering flow in wedge-shaped [4–8] and nonflat Hele-Shaw cells [9–13]; (ii) by putting the cell into motion, and rotating it around an axis perpendicular to the plane of the flow [14–16]; (iii) or even by studying the flow of more complex liquids such as non-Newtonian [17–20] and magnetic [21,22] liquids or by investigating pattern evolution in miscible fluids [23–29].

A particularly interesting variation of the traditional Saffman-Taylor problem is the investigation of fingering instabilities in Hele-Shaw cells presenting variable gap spacing [30–34,36]. In such a "lifting" version of the problem, the pressure gradient within the more viscous fluid is due to the lifting of the upper plate, while the lower plate remains at rest. Rectangular geometry flow in lifting cells has been studied in Refs. [30–32] where the upper plate is lifted just by one edge, making the gap both time and space dependent. A somewhat simpler radial geometry situation has been examined in Refs. [33,34,36], where the upper plate is lifted uniformly, i.e., the plates remain parallel to each other during the lifting process, so that the gap is a function of time, but not of space. This defines the so-called *time-dependent gap* Hele-Shaw cell. This uniform lifting makes the fluid-fluid interface move inward, forming visually striking fingering patterns. It is worth noting that fluid flow in lifting Hele-Shaw cells is not only intrinsically interesting, but also of significant importance to adhesion related problems [37–43]. In such types of problems the force and the energy required

*Email address: chingyao@yuntech.edu.tw
†Email address: jme@df.ufpe.br

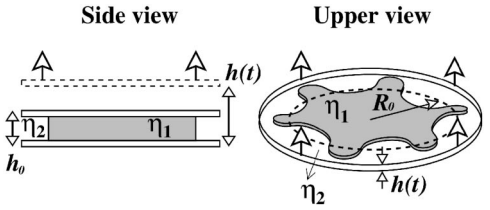

FIG. 1. Schematic representation of the time-dependent gap Hele-Shaw cell with miscible fluids.

to separate two adhesively bonded surfaces can be quite successfully evaluated through a Hele-Shaw approach (Darcy's law formulation).

Due to the practical and academic relevance of the lifting cell problem it is of interest to study and understand the emerging interfacial patterns under many different physical circumstances. To date, the totality of the lifting cell studies in the literature [30–34,36] consider flow of *immiscible* fluids, which inherently assumes the existence of a surface tension at the fluid-fluid interface. Conversely, in this paper we analyze the situation in which the fluids are *miscible*, and consequently present negligible interfacial tension. The question arises as to whether miscibility gives rise to any unusual interfacial shapes and behaviors. To address issues like this we perform intensive numerical simulations of the system and investigate how miscible displacements in a time-dependent gap Hele-Shaw cell may lead to interesting dynamical and morphological effects, particularly during advanced nonlinear stages of pattern evolution.

The layout of the rest of the paper is as follows. Section II formulates our theoretical approach and presents the governing equations of the time-dependent gap Hele-Shaw system with miscible fluids. Section III discusses the influence of key physical parameters on the development of miscible fingering in an originally circular droplet surrounded by a miscible, less viscous fluid. First, in Sec. III A we analyze the combined role played by diffusive effects and lifting rates (expressed by the dimensionless Péclet number Pe), viscosity contrast A (dimensionless viscosity difference between the fluids), and Korteweg stress parameter δ (effective surface tension for miscible flow [44–48]) in determining interfacial behavior. By examining the various simulated concentration images for the patterns important miscible interfacial features such as droplet recircularization and finger competition are identified and characterized. In the limit of high Pe, large A, and small δ a very interesting phenomenon is identified: the fingers pinch off and detached satellite droplets are formed. A tentative parallel of our results including Korteweg stresses and the immiscible case is also discussed. Subsequently, in Sec. III B a more quantitative analysis of the patterns is provided, with the help of two important quantities: interfacial mixing length and diameter of gyration. Our main conclusions are summarized in Sec. IV.

II. PHYSICAL PROBLEM AND GOVERNING EQUATIONS

The geometry of the lifting Hele-Shaw cell problem is schematically sketched in Fig. 1. We consider the miscible displacement and the development of interfacial instabilities when an initially circular fluid droplet of viscosity η_1 is surrounded by a less viscous fluid of viscosity η_2 in a time-dependent gap Hele-Shaw cell. We define our two-dimensional coordinate system in such a way that its origin is located at the center of the droplet. In this confined environment the flow takes place between two narrowly spaced flat plates, where the upper plate is lifted at a specified rate, and the lower plate is held fixed. During the lifting process the pressure gradient causes an inward viscous flow in the plane of the cell, leading to the formation of interfacial deformations. The initial plate spacing is represented by h_0, and at a given time t the plate-plate distance is denoted by $h=h(t)$. The radius of the initially circular droplet is denoted by $R_d(t=0)=R_0$. As in Refs. [33,41] we assume an exponentially increasing gap width $h(t)=h_0\exp(at)$, where a is a control parameter. This is precisely the ideal plate separation profile used in related adhesion probe-tack tests [41], since it provides a more uniform kinematics and nearly constant strain rate.

The dynamics of the incompressible miscible interface differs from the immiscible situation in two main aspects, i.e., the Korteweg stresses [44–48] and the velocity divergence [45–49]. Korteweg stresses arise as a result of concentration gradients at the interface between two miscible fluids, and may lead to dynamic surface-tension-like effects within areas of steep concentration gradients. The divergence effects are caused by the density variation of mixing. A recent study of miscible displacements in cylindrical tubes [49] has confirmed that such velocity divergence effects are insignificant; therefore we neglect them in the present simulations. Bouyancy effects are neglected as well.

Here we point out some important requirements and limitations of the Darcy's law formulation we employed in this work. First, as is common in Hele-Shaw systems [2,33], we consider that during the lifting process the system remains of large aspect ratio: the gap width h is always far smaller than a characteristic length scale in the plane of the cell, which we take as the droplet radius R_d, so that $R_d/h \gg 1$. This means that quantitative accuracy should be expected for times $t \ll (2/3a)\ln(R_0/h_0)$. A second important requirement refers to the fact that the velocity profile across the gap needs to remain parabolic [51,52]. Then we assume that the Taylor dispersion [50] is significant, so that the concentration gradients are not high across the gap. Also, recent results in density-driven flows [53–56] show that for high Rayleigh numbers, the Hele-Shaw equations might not be able to provide a completely accurate representation of the flow field, due to the extremely fine structures which are comparable to the gap width. Under these situations, the full three-dimensional Stokes equations or Brinkman model seem to be more appropriate to capture the instability features, such as the dominant wavelength.

Despite the restrictions described in the previous paragraph, we emphasize that the Darcy's law representation of the lifting cell problem with immiscible fluids has been used in numerous theoretical and experimental studies [31–34,36–43], always providing a pretty good description of both fingering dynamics and adhesion properties. This is nicely illustrated by the striking similarity between the nu-

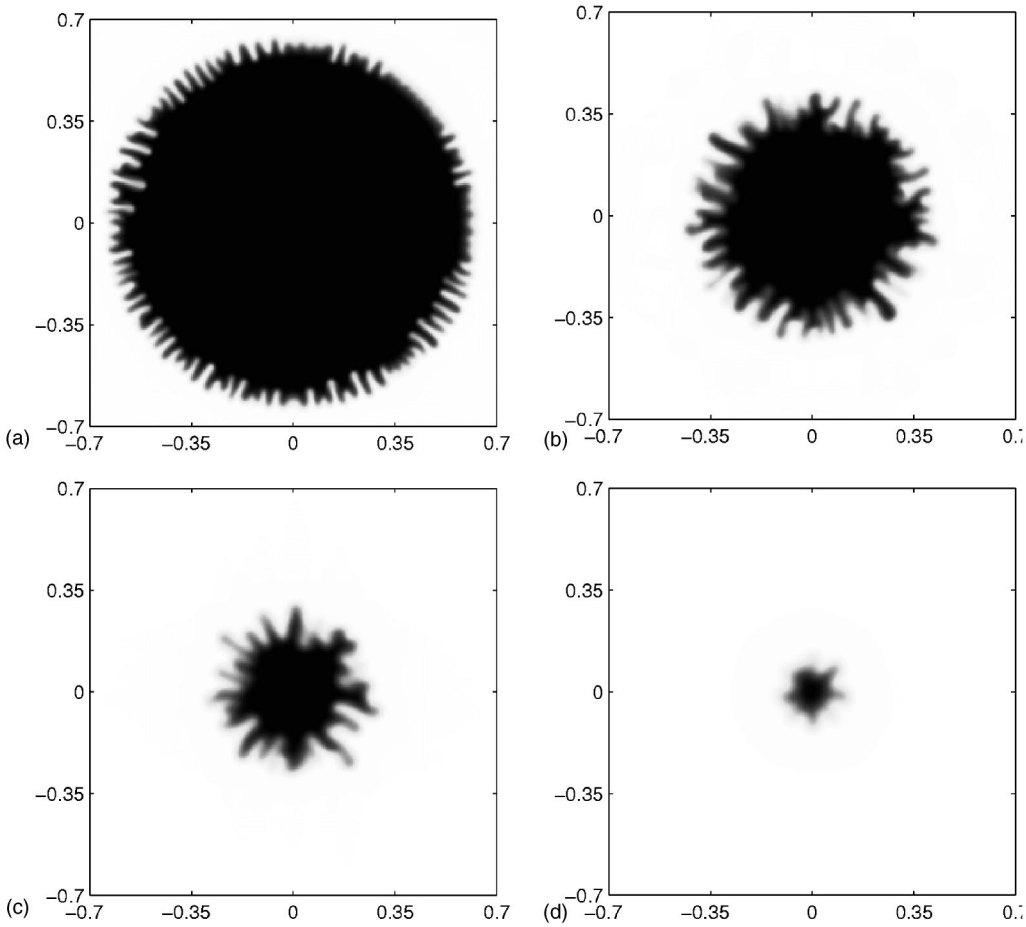

FIG. 2. Concentration images for $\mathrm{Pe}=4.0\times10^3$, $A=0.762$, and $\delta=0$ at $t=$ (a)1, (b)2, (c)3, and (d)5.

merical results of Shelley *et al.* [33] and the experimental investigations performed by Derks and co-workers [38]. The comparison between the results obtained in Refs. [33,38] demonstrates that the Darcy's law model accounts for the initial, intermediate, and fully nonlinear evolution of the observed fingering patterns. The evident success of the Darcy's law in describing the immiscible system motivated us to use this theoretical tool to study its miscible counterpart. In spite of the fact that to date there are *no* experimental studies with miscible fluids in lifting Hele-Shaw cells, our current Darcy's law approach seems to be quite promising as our numerical simulations compare quite well with the patterns found in Refs. [33,38], when the effects of Kortweg stress (effective surface tension) are introduced. Hopefully, this work will stimulate lifting Hele-Shaw experimental investigations with miscible fluids which would allow a check of our theoretical predictions.

Concerning some practical aspects of possible experiments with miscible fluids in lifting Hele-Shaw cells, one obvious setup would be to immerse the whole apparatus, already containing a confined droplet of the more viscous fluid surrounded with the less viscous one, in a recipient containing the less viscous fluid. Of course, this may represent an experimental challenge because the fluids may get mixed up before the lifting starts, or undesirable air bubbles can be trapped between the plates. Regarding the values of the physical parameters which could be used in such experiments, we point out that the values of the relevant dimensionless parameters Pe, A, and δ (defined below) used in our simulations are consistent with the typical values of physical parameters used in equivalent (and existing) experiments with immiscible fluids [38–41] and with well known values of the diffusion coefficient [47,57]. For example, with a typical initial lifting velocity $v=ah_0=O(10^{-7})$ m/s, initial gap width $h_0=O(10^{-4})$ m, and initial droplet radius $R_0=O(10^{-2})$ m as given in Ref. [38], the practical value of $\mathrm{Pe}=O(10^3)-O(10^4)$ is obtained, which is in the range we simulated. However, this happens under constant lifting speed conditions [38]. Another possible set of experimental data is given in Ref. [35]: they had applied a constant pressure, which also leads to an exponential speed profile. Within such circumstances a lifting speed correlation [Eq. (2) of Ref. [35]] is obtained which leads to a lifting coefficient $a=0.53$ in their experiments, resulting in $\mathrm{Pe}=O(10^5)-O(10^6)$, which is higher than the typical values of the Péclet number Pe we had used in our simulations. We mention that such a high Péclet number case is beyond the range of validity of our current numerical code. Finally, note that the thin film formulation we adopt imposes restrictions on the value of the lifting speed. A smaller lifting speed generally ensures the better applicability and accuracy of the thin film approach. Based on the experimental data of Refs. [35,38] we can es-

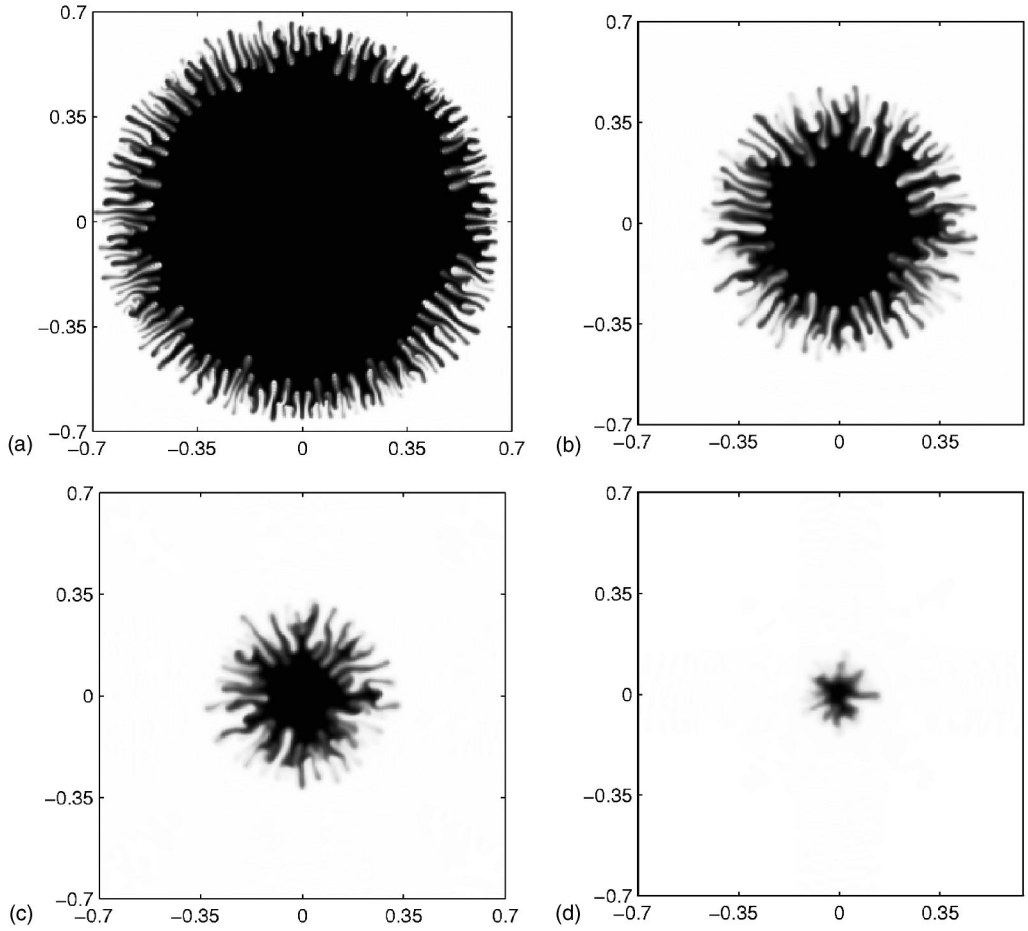

FIG. 3. Concentration images for $\mathrm{Pe}=1.2\times10^4$, $A=0.762$, and $\delta=0$ at $t=$ (a)1, (b)2, (c)3, and (d)5.

timate that, at least for a lifting coefficient $a<0.53$ [$\mathrm{Pe}=O(10^5)-O(10^6)$] for constant pressure, or for constant speed $v<8.73\times10^{-7}$ m/s [$\mathrm{Pe}=O(10^4)$], the situations still fit quite well with the predictions of our present numerical Hele-Shaw formulation.

The dynamical evolution in a time-dependent gap Hele-Shaw cell is governed by the following equations [25,27,32,33,47]:

$$\nabla\cdot\mathbf{u}=-\frac{\dot{h}(t)}{h(t)}, \tag{1}$$

$$\nabla(p+Q)=-\frac{12\eta}{h^2}\mathbf{u}+\nabla\cdot[\hat{\delta}(\nabla c)(\nabla c)^T], \tag{2}$$

$$\frac{\partial c}{\partial t}+\mathbf{u}\cdot\nabla c=D\nabla^2 c. \tag{3}$$

Equation (1) expresses a modified incompressibility condition which accounts for the lifting of the upper plate [32,33]. The gap averaged velocity is $\mathbf{u}$, while the overdot denotes total time derivative. A generalized Darcy's law is expressed by Eq. (2) where p is the hydrodynamic pressure, and Q is the additional pressure due to the Korteweg stresses [25,47]. The concentration of the fluid 1 is represented by c, and $\hat{\delta}$ is the Korteweg stress coefficient. The superscript T denotes a transpose. The concentration equation is given by Eq. (3), where D is the constant diffusion coefficient.

The viscosity variations of the mixture are assumed as [23,24]

$$\eta(c)=\eta_1\exp[R(1-c)], \tag{4}$$

where $R=\ln(\eta_2/\eta_1)$ is a viscosity parameter. In order to render the governing equations (1)–(4) dimensionless, the radius of the initial circular droplet R_0 is used as the characteristic length scale. We further scale the viscosity with η_1 and time with $1/a$. In conjunction with the characteristic velocity aR_0 and pressure $(12\eta_1 aR_0{}^2)/h_0{}^2$, dimensionless governing equations are obtained:

$$\nabla\cdot\mathbf{u}=-1, \tag{5}$$

$$\nabla(p+Q)=-\frac{\eta}{e^{2t}}\mathbf{u}+\nabla\cdot[\delta(\nabla c)(\nabla c)^T], \tag{6}$$

$$\frac{\partial c}{\partial t}+\mathbf{u}\cdot\nabla c=\frac{1}{\mathrm{Pe}}\nabla^2 c, \tag{7}$$

$$\eta(c) = \exp[R(1-c)]. \tag{8}$$

The dimensionless parameters, such as the Péclet number Pe, the viscosity contrast (or the Atwood viscosity ratio) A, and the Korteweg constant δ are defined as

$$\mathrm{Pe} = \frac{aR_0^{\ 2}}{D}, \quad A = \frac{1-e^R}{1+e^R}, \quad \delta = \frac{\hat{\delta} h_0^2}{12\eta_1 a R_0^4}.$$

The velocity is split into a divergence-free component $\mathbf{u}_f$ which is the velocity of the constant gap spacing case, and an axisymmetric divergent radial velocity $\mathbf{u}_d = \mathbf{u}_d(r)$ caused by the gap variation, so that

$$\mathbf{u} = \mathbf{u}_f + \mathbf{u}_d, \tag{9}$$

$$\boldsymbol{\nabla} \cdot \mathbf{u}_f = 0, \tag{10}$$

$$\boldsymbol{\nabla} \cdot \mathbf{u}_d = -1. \tag{11}$$

The divergent radial velocity is obtained directly from Eq. (11) as $\mathbf{u}_d = -\mathbf{r}/2$, which is a potential field. On the other hand, by rewriting the momentum equation (2) in the stream function ϕ and vorticity ω formulation, the divergence-free component $\mathbf{u}_f$ can be obtained by solving the equations [24,29,47]

$$u_f = \frac{\partial \phi}{\partial y}, \quad v_f = -\frac{\partial \phi}{\partial x}, \tag{12}$$

$$\nabla^2 \phi = -\omega, \tag{13}$$

$$\omega = -R\left[u\frac{\partial c}{\partial y} - v\frac{\partial c}{\partial x}\right] - \frac{e^{2t}\delta}{\eta}\left[\frac{\partial c}{\partial x}\left(\frac{\partial^3 c}{\partial x^2\,\partial y} + \frac{\partial^3 c}{\partial y^3}\right) - \frac{\partial c}{\partial y}\left(\frac{\partial^3 c}{\partial x\,\partial y^2} + \frac{\partial^3 c}{\partial x^3}\right)\right]. \tag{14}$$

As to the boundary conditions, the nonvanishing divergence-free stream function given by Eq. (14) is induced by concentration gradients. Consequently, for regions located outside the droplet (where no concentration gradient is present), the stream function is zero. Therefore, the choice of computational domain is arbitrary as long as the domain contains the whole droplet. Of course, the divergent radial component is still present within the entire computational domain. In this study, we choose the boundaries to vary between $+4/3$ and $-4/3$ in both x and y directions. Under such circumstances, the boundary conditions are prescribed as follows

$$\phi = 0, \ \frac{\partial c}{\partial x} = 0 \quad \text{for } x = \pm\frac{4}{3}, \tag{15}$$

$$\phi = 0, \ \frac{\partial c}{\partial y} = 0 \quad \text{for } y = \pm\frac{4}{3}. \tag{16}$$

In order to reproduce the very fine structures of the fingers successfully, a highly accurate spectral method is applied. As a result, the actual boundary conditions applied in the numerical codes at $x = \pm 4/3$ are modified as $\partial\phi/\partial x = 0$. Under the present situation where no concentration gradient is generated on these boundaries before the calculations terminate, the above conditions automatically lead to $\phi = 0$. The initial conditions assume a circular droplet shape bounded by a steep concentration gradient in the form of an error function. To break the unphysical artificial symmetry, a small magnitude of random noise is applied to the positions of 0.5 concentration. To solve the stream function Eq. (13) by a pseudospectral method, a Galerkin-type discretization using a cosine expansion is employed in the streamwise direction on both ω and ϕ. In the normal direction, discretization is accomplished by sixth order compact finite differences. The vorticity equation (14) is evaluated by sixth order compact finite difference schemes. A fully explicit third order Runge-Kutta procedure on time and spatial sixth order compact finite difference schemes are employed to solve the concentration Eq. (7). The set of equations is then solved and advanced in time. The numerical code is similar to the one used for earlier investigations of miscible flow in other geometries [24–27], and is quantitatively validated by comparing the growth rates with the values obtained from the linear stability theory in a plane front. More details on the implementation and quantitative validation of these schemes are provided by Refs. [27–29].

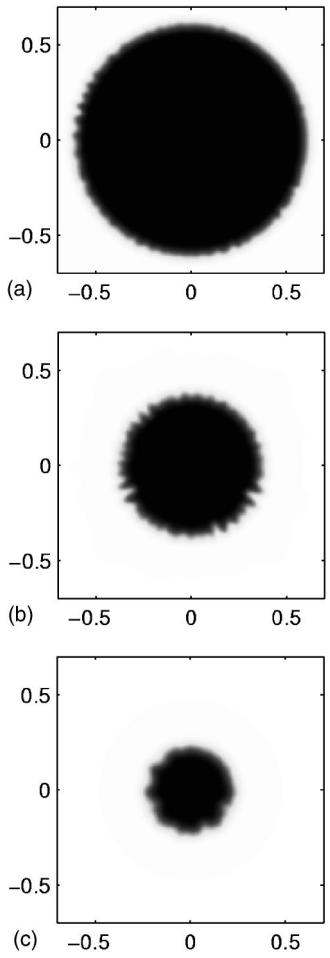

FIG. 4. Concentration images for $\mathrm{Pe} = 2.0 \times 10^3$, $A = 0.762$, and $\delta = 0$ at $t =$ (a)1, (b)2, and (c)3.

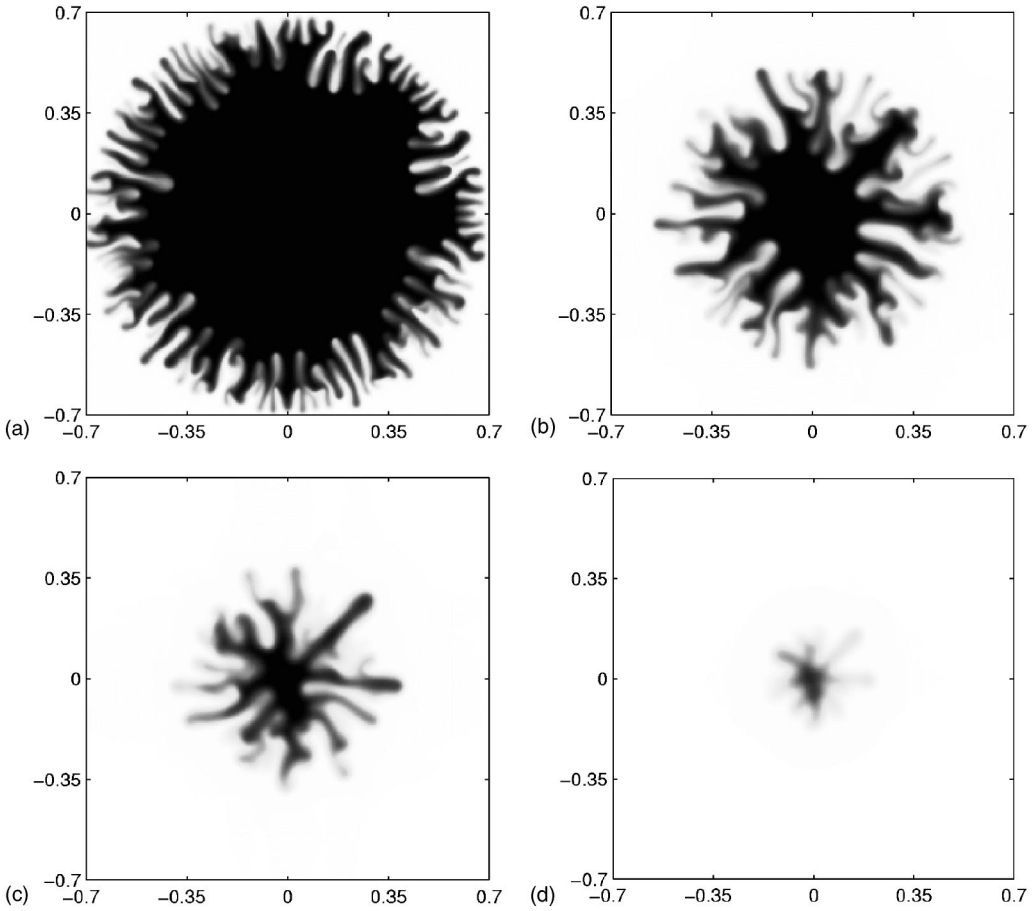

FIG. 5. Concentration images for $\mathrm{Pe}=4.0\times10^3$, $A=0.905$, and $\delta=0$ at $t=$ (a)1, (b)2, (c)3, and (d)5.

III. RESULTS AND DISCUSSION

This section is divided in two parts. Section III A presents the actual interfacial patterns obtained by our numerical study, and examines the combined influence of diffusive, viscous, and Korteweg stress effects on their evolution and shape. Section III B provides a more quantitative account of the morphological features shown in Sec. III A, where interesting phenomena related to recircularization of the more viscous droplet and finger competition behavior have been initially discussed.

A. Influence of diffusive, viscous, and Korteweg stress effects

The beautiful interfacial patterns obtained for *immiscible* displacement in lifting Hele-Shaw cells have been investigated by both experiments [30,31,34,38–41] and numerical simulations [33]. In these studies it is found that during the lifting process the initially circular droplet of the fluid 1 goes through basically three different stages. (i) The first one is characterized by the rapid ramification of the interface via the penetration of multiple fingers of the outer, less viscous fluid 2 into fluid 1. These inward fingers become progressively thicker and acquire rounder shapes as time progresses. (ii) Following the initial period of intense instability and ramification, a second stage arises in which the number of fingered structures diminishes, indicating that the instability cannot be sustained indefinitely. (iii) In a final stage, one particularly interesting phenomenon takes place, making the droplet shrink and recircularize. The numerical simulations for the immiscible case [33] also show that increasingly smaller values of surface tension lead to stronger interface ramification, resulting in a delayed recircularization process. We point out that the accurate numerical description of the zero surface tension flow in the immiscible case is a challenging problem: when surface tension vanishes the interface begins to sharpen, and the spatial Fourier spectrum broadens rapidly, quickly exhausting the available resolution.

Interestingly, the lifting Hele-Shaw cell investigations performed so far focus solely on the *immiscible* case, and in addition, just consider the *high* viscosity contrast limit ($A=1$). Therefore, the interplay between viscous and diffusive effects for similar flows involving *miscible* fluids is still largely unexplored in the present literature. One noteworthy point about miscible flows is the fact that interfacial tension is actually negligible. Due to the smooth character of the diffusive effects involved, the study of miscible interfaces may provide a nice and easier way to access complicated immiscible flow circumstances in which surface tension vanishes [33]. Suggestive interfacial behaviors like droplet recircularization and finger competition can be revisited and further analyzed in the miscible case. The occurrence of some other important interfacial features, not yet fully examined in the immiscible time-dependent gap situation, such as finger

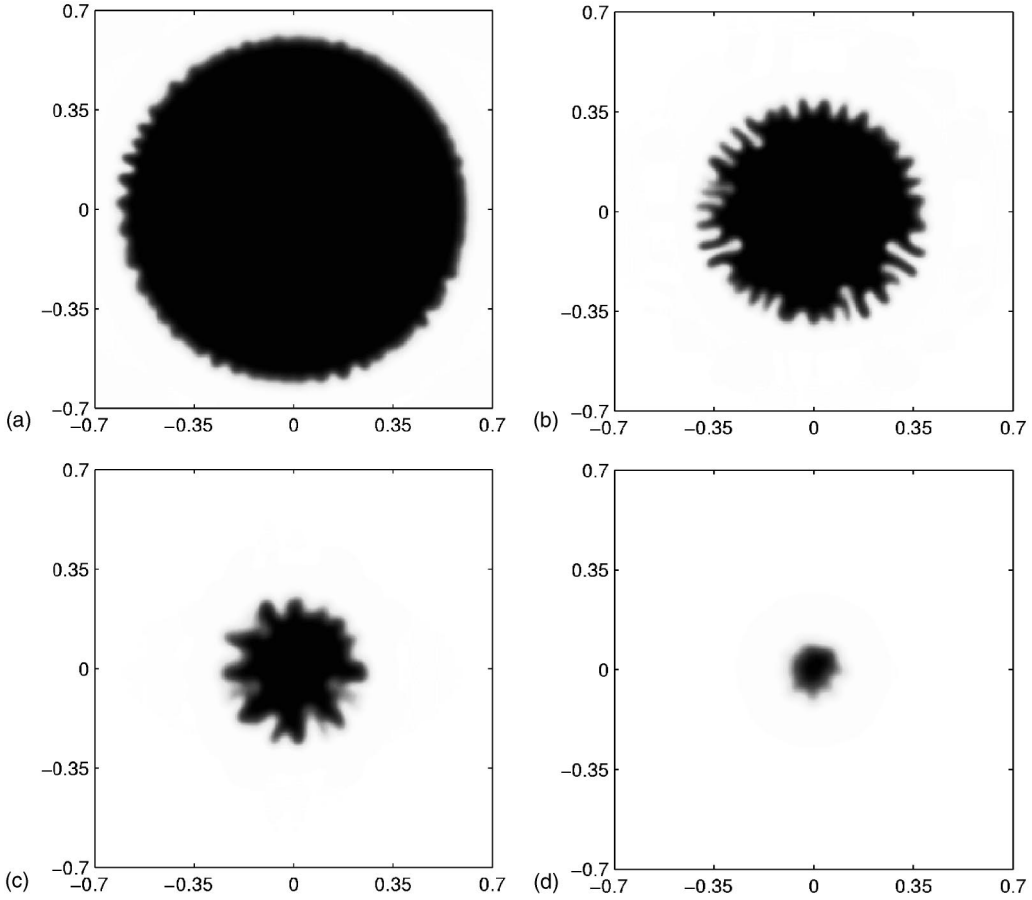

FIG. 6. Concentration images for $\mathrm{Pe}=4.0\times10^{3}$, $A=0.762$, and $\delta=-5.0\times10^{-7}$ at $t=$ (a)1, (b)2, (c)3, and (d)5.

pinch-off and droplet detachment could be studied as well. Moreover, it is also worth investigating the possibility of reintroducing surface-tension-like effects into the miscible case, through the action of Korteweg stress. So a thorough investigation of the relationship between miscibility and the fluid-fluid interface dynamics still needs to be addressed in lifting Hele-Shaw cells. In this work we begin such investigations, focusing on the problem involving Newtonian, nonmagnetic miscible fluids.

We begin our numerical investigation performing a systematic study of the concentration images obtained for different values of the relevant control parameters, the Péclet number Pe, viscosity contrast A, and Korteweg stress δ. Figure 2 depicts the sequential images of concentration for a representative case with $\mathrm{Pe}=4.0\times10^{3}$, $A=0.762$, but assuming absence of Korteweg stress, so that $\delta=0$. At the earlier stage $t=1$, one can observe the appearance of peculiar fingering instabilities at the fluid-fluid border mostly due to viscous effects (here the inner fluid 1 is about 7.4 times more viscous than the surrounding fluid 2). One striking morphological difference with the immiscible case can be already detected at this early stage, which presents the development of a *large* number of very *thin* fingers. As time progresses the vigorous fingering process keeps evolving up to $t=2$, revealing interesting nonlinear behaviors, such as finger merging and a sort of tip splitting of the outgoing more viscous fingers. However, we notice that the shrinking interface at later time period limits the further growth of the fingers, so that the instability is found less significant after $t=3$. Actually, only a few dispersed fingers are left at $t=5$. Note that only at this very late stage does the fingering pattern begin to show some tendency toward recircularization. This last finding seems to indicate that miscibility would tend to delay or inhibit the recircularization process. This is consistent with the numerical observations of Ref. [33] for the immiscible case which pointed to less tendency to droplet recircularization for lower values of surface tension.

In Fig. 3 we keep the same physical parameters used in Fig. 2, but now increase the value of the Péclet number to $\mathrm{Pe}=1.2\times10^{4}$, meaning weaker diffusive effects or faster lifting rates. At this point, we stress the fact that the initial conditions are exactly the same for all patterns simulated in this work. In Fig. 3 we observe the enhancement of fingering instabilities at early stages ($t=1$), with the formation of even higher number of fingers, and the development of more vigorous branching events at $t=2$, 3. Note that even at $t=5$ some well defined fingered structures still survive, so that stabilization and recircularization are not yet fully achieved. For this higher value of Pe the patterns obtained are markedly different from the ones typically found in the corresponding immiscible situation [33,38]. Here the interface is much more ramified, presenting outgoing fingers which develop a peculiar forklike or tridentlike shape. On the other hand, if the Péclet number is lowered to $\mathrm{Pe}=2.0\times10^{3}$ as shown in

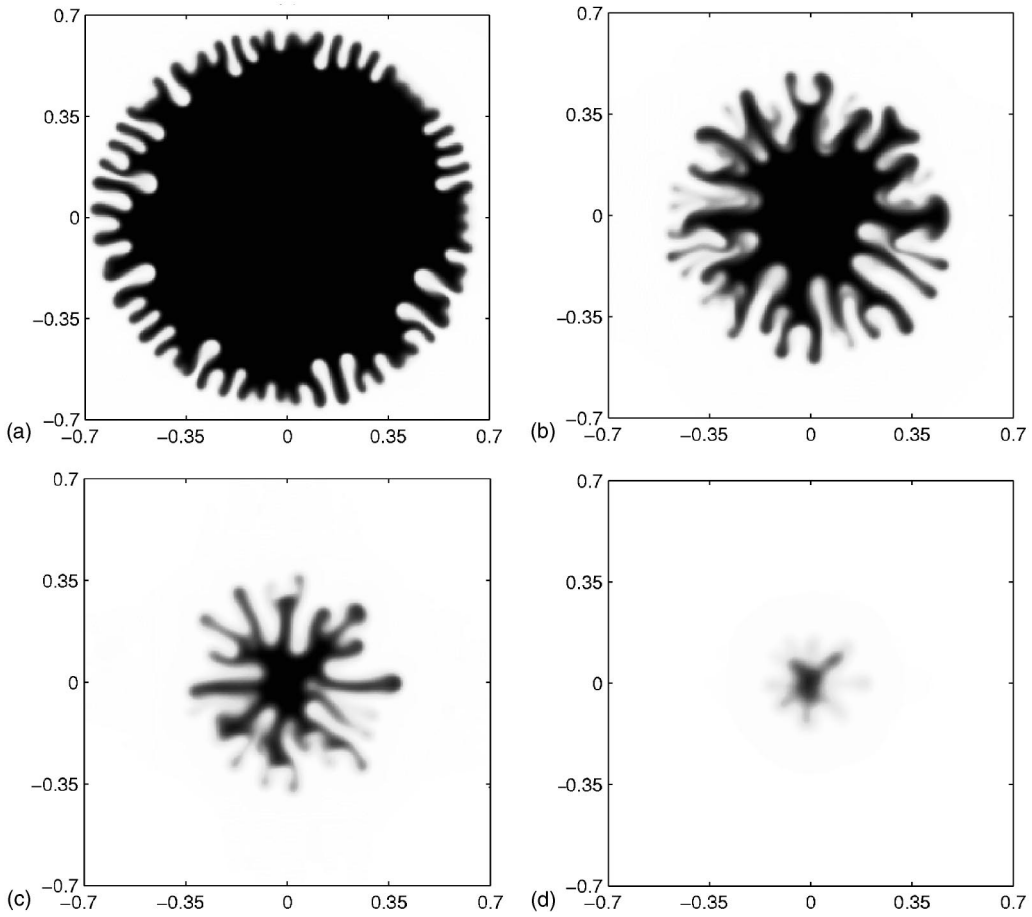

FIG. 7. Concentration images for $\mathrm{Pe}=4.0\times10^3$, $A=0.905$, and $\delta=-5.0\times10^{-7}$ at $t=$ (a)1, (b)2, (c)3, and (d)5.

Fig. 4, one can clearly see that the instabilities are significantly dampened, resulting in a much smoother shrinking interface. In this respect, we have verified that for the situation in which $\mathrm{Pe}=10^3$ the contracting droplet remains nearly circular during the whole lifting process.

Now we turn to the investigation of the role played by the viscosity contrast A. As in Fig. 2, we keep the Péclet number fixed at $\mathrm{Pe}=4.0\times10^3$ and still set $\delta=0$, but now allow variations in the viscosity contrast. In agreement with the conventional viscous fingering problem [1–3], less fingering is detected at lower values of A. At a lower viscosity contrast $A=0.462$, the shrinking interface is further stabilized, and no apparent instability is induced. Also in line with the usual Saffman-Taylor problem [1–3], Fig. 5 illustrates that more vigorous fingering is triggered at a higher viscosity contrast $A=0.905$. One curious point is the rising of curly side-branching structures in some fingers ($t=2$). It is also interesting to notice the fundamental differences regarding the enhanced fingering processes induced by Péclet number (Fig. 3), and viscosity contrast (Fig. 5). In Fig. 5 it is clear that initially ($t=1$) the fingers are a bit thicker, and appear in smaller number in comparison to the structures obtained in Fig. 3. In addition, note that for later times ($t=3$), the patterns formed in Fig. 5 present outgrowing fingers which are significant longer than the ones obtained in Fig. 3.

The fingering instabilities at higher Péclet numbers (Fig. 3), which provide stronger concentration gradient locally, are mostly produced by the inward motion of the less viscous fingers penetrating the more viscous fluid. This motion occurs in such a way that the relative lengths of the less viscous fingers do not differ very much, making their tips to define an approximately circular internal region in the more viscous fluid, as typically shown in Fig. 3. In other words, for higher Pe the length variability among the inward fingers is not too pronounced, which characterizes patterns with a relatively well preserved internal circular region of the more viscous fluid. In contrast, as illustrated in Fig. 5, a higher viscosity contrast leads to a more significant and less uniform penetration of the less viscous inward fingers, originating structures that compete more strongly with each other, resulting in an array of incoming fingers presenting a variety of lengths. Consequently, for higher A the internal region of the more viscous fluid is not typically circular in shape. A similar type of behavior, at high viscosity contrast, is also observed for miscible flow in Hele-Shaw cells presenting different geometries [24]. More quantitative descriptions regarding the different mechanisms of pattern evolution and finger competition for higher values of Pe or A are provided in Sec. III B.

We close this section by discussing the role played by Korteweg stresses [44–48] for confined flow in a time-dependent gap Hele-Shaw cell. Both numerical [25,27] and

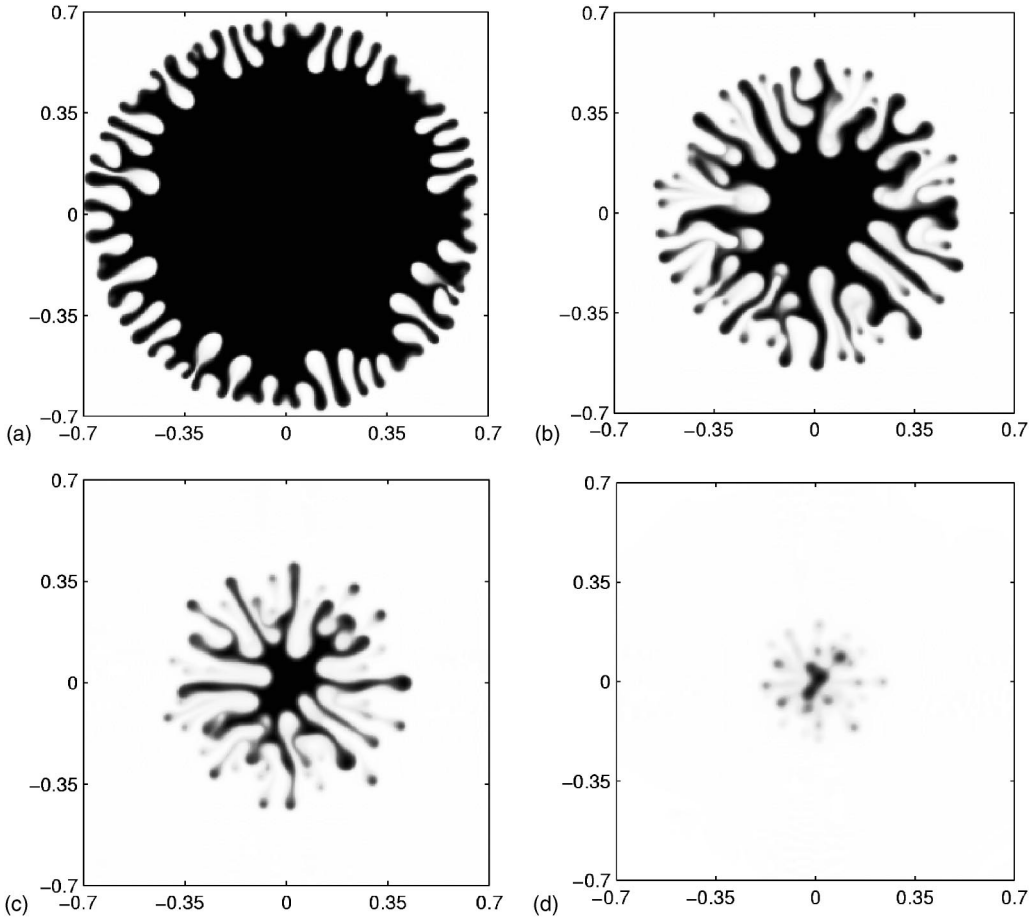

FIG. 8. Concentration images for $\mathrm{Pe}=1.2\times10^4$, $A=0.905$, and $\delta=-5.0\times10^{-7}$ at $t=$ (a)1, (b)2, (c)3, and (d)5.

analytical investigations [47] of miscible flow systems including Korteweg stresses have found interesting morphological similarities between the observed miscible patterns and the structures obtained in related immiscible flows. This resemblance suggests the possibility of seeing Korteweg stresses as a sort of effective surface tension for the miscible case. As pointed out in Ref. [47], a meaningful interpretation of Korteweg stresses as an effective surface tension in Hele-Shaw flows requires the use of *negative* values of Korteweg stress constant δ, otherwise the problem would be ill posed.

The action of the Korteweg stresses on the pattern evolution is initially shown in Fig. 6 for $\mathrm{Pe}=4.0\times10^3$, $A=0.762$, and $\delta=-5.0\times10^{-7}$. The pattern obtained in Fig. 6 reveals the stabilizing role played by the Korteweg stresses, in the sense that interfacial instabilities are significantly restrained. The latter can be clearly verified by comparing the patterns shown in Fig. 6 (for $\delta\neq0$) with those obtained in Fig. 2 which used the same physical parameters, but assumed $\delta=0$. In particular, we point out the pattern shown in Fig. 6(b) ($t=2$) is very similar to the ones commonly obtained in the corresponding immiscible situation [33,38]. We have also verified that a fully stable circular front is recovered for stronger Korteweg constant at $\delta=-10^{-5}$. These results are in accordance with the findings of Refs. [25,27], which reported Korteweg-stress-induced stabilization for Hele-Shaw cells with different flow geometries.

Figure 7 illustrates pattern evolution for higher values of the viscosity contrast: now $A=0.905$, $\delta=-5.0\times10^{-7}$, and $\mathrm{Pe}=4.0\times10^3$. In contrast to the similar case depicted in Fig. 5 in which Korteweg stresses are neglected, now we see that the initial patterns ($t=1$) exhibit a smaller number of inward fingers, which are thicker and present much more rounded tips. Actually, the most noteworthy fact is the resemblance of these initial miscible patterns with the ones normally obtained for immiscible flow in lifting Hele-Shaw cells [33,38]. Again, this result for time-varying gap Hele-Shaw cells reinforces the claim that Korteweg stresses do act like an effective surface tension for miscible flow [25,27]. Of course, the shape similarity between these miscible and immiscible patterns also provides an indirect validation of our current miscible simulations. Finally, as time advances in Fig. 7 ($\delta\neq0$) we see that, despite the large value of A, the resulting interfacial patterns are not as intricate as those obtained in Fig. 5 ($\delta=0$), a stabilizing effect obviously induced by Korteweg stresses.

Explorations of the coupling effects for even higher Pe $=1.2\times10^4$ at $A=0.905$ and $\delta=-5.0\times10^{-7}$ are also conducted, as shown in Fig. 8. The increase in the value of the Péclet number provides stronger concentration gradients that enhance finger penetration. This finding is easily verified by comparing Figs. 7 and 8 at $t=1$. As a result, extremely slim fingers are resulted by current high Pe and A. This strong finger penetration process, associated with transverse diffusion, leads to the striking phenomenon of finger pinch-off, and eventually to the detachment of droplets at the finger

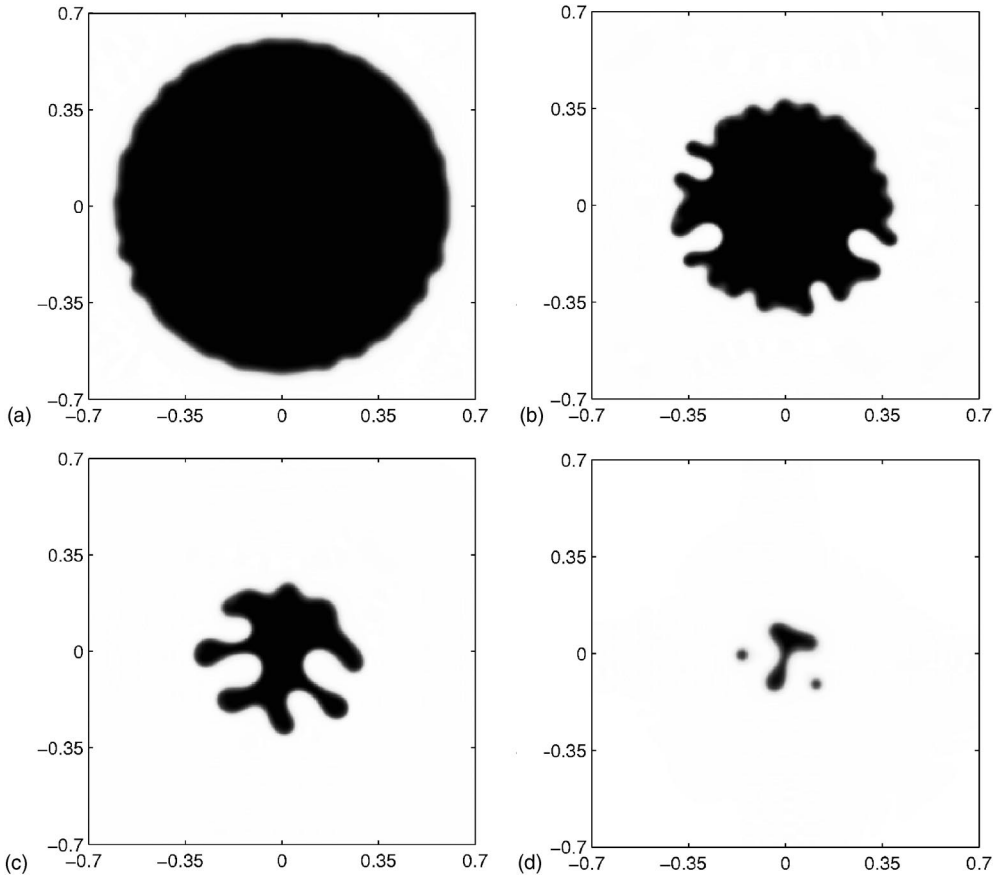

FIG. 9. Concentration images for $\mathrm{Pe}=1.2\times10^{4}$, $A=0.905$, and $\delta=-2.5\times10^{-6}$ at $t=$ (a)1, (b)2, (c)3, and (d)5.

tips. Numerous tiny droplets are formed throughout the lifting process after $t=1$. We point out that finger pinch-off and droplet emission have also been recently detected in experiments for *immiscible* flow in *rotating* Hele-Shaw cells [16] in the limit of *low* viscosity contrast and *low* surface tension.

It is interesting to notice that the droplet detachment phenomena we detected in our current miscible case for relatively large values of Pe and A has not been reported in similar immiscible flows in lifting Hele-Shaw cells [33,38]. This fact can be attributed to the different mechanisms of droplet detachment involved in immiscible and miscible flows. While the detachment in immiscible situations indicates the occurrence of interfacial singularities, it occurs much more smoothly in miscible cases due to diffusive effects. So, despite going through several "near-pinching" situations for immiscible flow in time-dependent gap cells [33], the simulated patterns for nonzero surface tension and $A=1$ are eventually reduced to a final circle, without exhibiting any droplet detachment at all. These numerical results for the immiscible case [33] agree with adhesion experiments in lifting cell geometry [38].

Numerical simulations for the immiscible case [33] also suggest possible singular behavior (droplet pinch-off) with harder driving, or with different initial conditions, even if surface tension is nonzero (typical immiscible case). It is also found that pinch-off would be favored when surface tension effects are sufficiently weak. Indeed, it is quite well known for immiscible flows that the addition of surface tension removes (regulates) interfacial singularities. In this sense, for the present miscible pinch-off case with harder driving (or higher Pe), and A near 1, but with very weak effective surface tension (Korteweg stresses) $\delta=-5.0\times10^{-7}$, the detachment of droplets could be somewhat expected. On this basis, it is of interest to investigate more closely how Korteweg stresses could influence the droplet detachment process.

In order to further clarify the effects of ersatz interfacial tension for Korteweg stresses, simulations at larger $\delta=-2.5\times10^{-6}$ and -5.0×10^{-6} are shown in Figs. 9 and 10, respectively. It is evident that a higher δ not only stabilizes the interface, but also restrains the occurrence of droplet detachment. From Fig. 9 we verify that initially ($t=1$) the interface presents just some small bumps, followed by the penetration of a few inward (wide and rounded) fingers ($t=2$, 3). In addition, we see that finger pinch-off is significantly weakened for $\delta=-2.5\times10^{-6}$. No droplet detachments are observed till $t=4$, when just two identifiable detached droplets are generated [see also Fig. 9(d)]. So it is evident that the detachment process is considerably delayed by the action of larger Korteweg stresses. On the other hand, from Fig. 10 we observe that droplet detachment is totally prevented by sufficiently larger values of Korteweg stresses $\delta=-5.0\times10^{-6}$. In addition, the droplet is fully recircularized after $t=6$. These findings provide an additional confirmation that Korteweg stresses indeed mimic surface tension for miscible

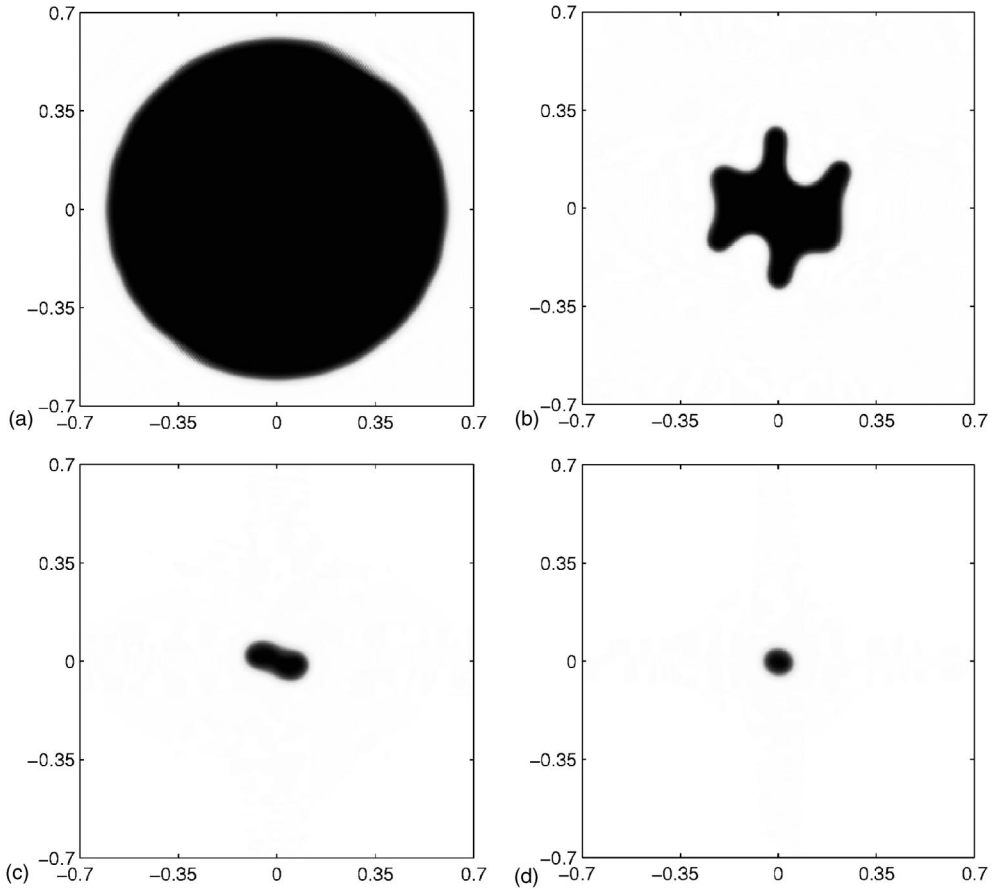

FIG. 10. Concentration images for $\mathrm{Pe}=1.2\times10^{4}$, $A=0.905$, and $\delta=-5.0\times10^{-6}$ at $t=$ (a)1, (b)3, (c)5, and (d)6.

flows: the interface is stabilized and the occurrence of finger pinch-off is suppressed. Finally, we point out that the patterns depicted in Figs. 9 and 10 again show great resemblance to the corresponding immiscible ones [33].

B. Recircularization and finger competition dynamics: A more quantitative analysis

After the analysis of the most relevant morphological features of the miscible displacement in time-dependent gap cells, which were based on concentration images (Sec. III A), we now present a more quantitative study of the patterns obtained. As in immiscible situations, the magnitudes of the fingering instabilities can be determined by the growth of a characteristic quantity related to the perimeter of the interface, the so-called mixing interfacial length L. However, unlike the immiscible case in which a sharp interface separating the fluids can be defined, the mixing region between miscible fluids is not a clear boundary, but rather a diffuse layer. So, strictly speaking no completely accurate interfacial length can be measured. Nevertheless, in the region of significant concentration gradient, the mixing length can be well represented as [24–26]

$$L=\int_{S}\sqrt{\left(\frac{\partial c}{\partial x}\right)^{2}+\left(\frac{\partial c}{\partial y}\right)^{2}}\,dx\,dy, \tag{17}$$

where S is the entire computational domain. On the condition of a stable circular immiscible interface, referred as the base state herein, the time-dependent interfacial length L_B due to lifting can be obtained as $L_B=2\pi\exp(-t/2)$. In general, the interfacial length starts to increase once the fingering instability is triggered; therefore an earlier growth and higher growth rate of interfacial length reflect a more unstable interface.

The interfacial lengths L for several values of Pe, A, and δ as well as the base state are shown in Fig. 11(a). For the cases presenting vigorous fingering, such as $\mathrm{Pe}\geqslant4.0\times10^{3}$, $A\geqslant0.762$, and $\delta\leqslant-5.0\times10^{-6}$, initially L increases sharply, reaches a maximum value, and then drops abruptly. This behavior is attributed to the stabilizing effect caused by the shrinkage of the interface. For the situations not involving significant fingering, i.e., $\mathrm{Pe}=10^{3}$ and $A=0.762$, the interfacial lengths behave quite similarly to the base state during the whole lifting process, presenting a nearly exponential decay.

Moreover, by inspecting Fig. 11(a) we notice that eventually all curves converge to the base state. Since the shrinkage of the droplet leads to the decay of interfacial length even in an unstable situation, the magnitude of the emerging fingering patterns can be conveniently described by the *normalized* interfacial length, defined as $L_n=L/L_B$ [see Fig. 11(b)]. The nice collapse of normalized interfacial length for $\mathrm{Pe}=10^{3}$ and $A=0.762$ not only confirms the stable situation as shown by concentration images in Sec. III A, but also validates the propriety of the representation of interfacial length by the present approximation. It is interesting to notice that, except

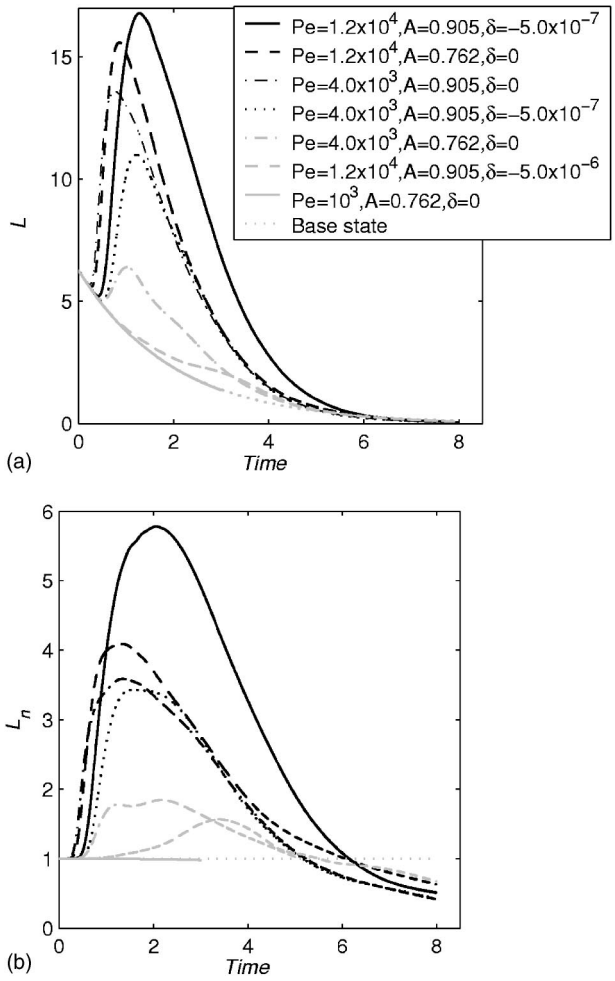

FIG. 11. Time evolution of interfacial length for various control parameters: (a) interfacial lengths L and (b) normalized interfacial lengths L_n.

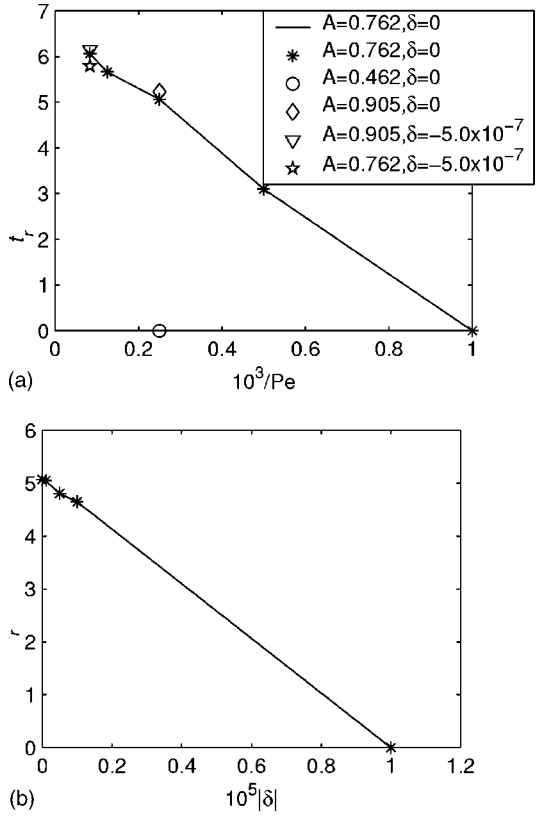

FIG. 12. Recircularization time t_r for (a) various Pe, and (b) various δ, $\mathrm{Pe}=4.0\times10^3$, and $A=0.762$.

for the strongest Korteweg stresses case with $\delta=-5.0\times10^{-6}$, longer interfacial lengths are mainly observed for larger Pe ($\mathrm{Pe}=1.2\times10^4$). Also confirmed quantitatively is the fact that more vigorous fingering occurs for higher Péclet number Pe, larger viscosity contrast A, or weaker Korteweg stresses δ, as the corresponding curves for L_n show more significant deviation from the base state.

Although the concept of mixing interfacial length given by Eq. (17) provides a good quantitative measurement of the strength and complexity of fingering patterns, it is certainly more reliable within the region with relatively strong concentration gradients. For the situation studied in this work, significant dispersion occurs throughout the entire droplet at late stages, when its area is small. Thus, Eq. (17) might not be entirely appropriate for an accurate representation of the interfacial length at very late stages of the lifting process. In particular, it may lead to inaccurate (underestimated) values of normalized interfacial lengths, such as that for later times $L_n<1$, illustrated in Fig 11(b).

Nevertheless, the measurements using Eq. (17) shown in Fig. 11(b) give correct trends regarding the stabilizing effects for different control parameters, and most importantly, provide a quantitative verification of the interesting droplet recircularization phenomenon discussed previously. Based on the concept of interfacial lengths, the recircularization time t_r can be defined as the time for which the normalized interfacial length L_n converges to unity. By observing Fig. 11(b) we conclude that longer recircularization times (which are associated to more unstable interfaces) are obtained at higher Péclet numbers, larger viscosity contrast, and weaker Korteweg stresses. The recircularization times t_r for various cases presented in this work are also plotted in Figs. 12(a) and 12(b). In Fig. 12 it is interesting to notice that t_r follows a nearly linear relationship with the inverse of the Péclet number $1/\mathrm{Pe}$, and with the absolute value of Korteweg parameter $|\delta|$, while it only depends weakly on viscosity contrast $A\geqslant0.726$.

Another important interfacial behavior that can be studied more quantitatively is the one related to different morphological interfacial features induced by higher Péclet number or higher viscosity contrast. As described in more qualitative terms in Sec. III A, a higher Pe leads to more fingering around a nearly circular region, while higher A leads to enhanced fingering around noncircular internal regions, due to stronger penetration of inward less viscous fingers. In order to verify the accuracy of these different mechanisms more quantitatively, the measurement of another auxiliary quantity is proposed. The one-dimensional profile of averaged concentration c_a across the width of the cell (y direction) can be obtained as [25]

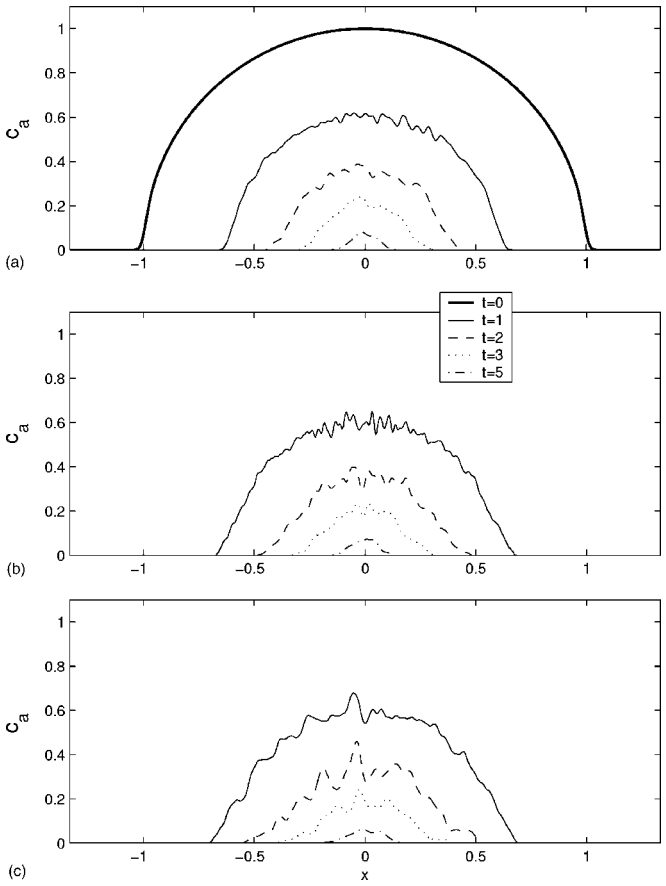

FIG. 13. Time evolution of averaged concentration profiles for $\delta=0$ at (a) $\mathrm{Pe}=4.0\times10^3$ and $A=0.762$, (b) $\mathrm{Pe}=1.2\times10^4$ and $A=0.762$, and (c) $\mathrm{Pe}=4.0\times10^3$ and $A=0.905$.

$$c_a(x)=\int_0^{4/3} c(x,y)dy. \tag{18}$$

Various profiles of the averaged concentration are plotted in Fig. 13. The initial profile appears in a semicircular shape as shown in Fig. 13(a) for the representative case, and shrinks as time proceeds. At later times, the rising of interfacial fingerings makes the profile fluctuate and deform. The nicely semicircular profile is no longer preserved. While a higher $\mathrm{Pe}=1.2\times10^4$ mainly leads to a larger number of fluctuated waves as shown in Fig. 13(b), more significant stretching and larger amplitudes are resulted by a stronger viscosity contrast $A=0.905$ in Fig. 13(c). The stretching of averaged profile provides an additional possible measurement to describe the behavior of the fingering patterns. To conserve mass or area in the present cases, stronger inward penetrations of the less viscous fingers in general induce more significant outward growth of the more viscous ones. As a result of such a process, the stretching of the averaged profile is expected to increase more significantly for stronger length variability of inward fingers. On the other hand, fingering around an approximately circular area affects this stretching weakly. In this sense, a quantity defined as diameter of gyration D_g, taken as the distance between the points at which $c_a=0.01$, could be used to probe in a more quantitative way the different morphological behaviors induced by larger Pe and larger A. Again, on the condition of a stable immiscible circular interface, the base state diameter of gyration D_{g_B} can be obtained, and the corresponding *normalized* diameter of gyration defined as $D_{g_n}=D_g/D_{g_B}$.

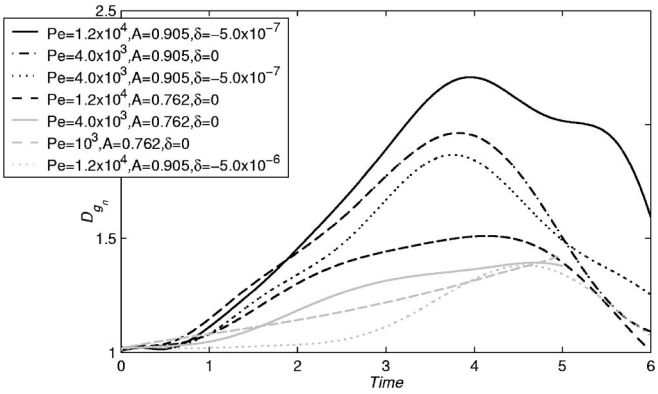

FIG. 14. Time evolution of normalized diameters of gyration D_{g_n} for various parameters.

Figure 14 depicts the time evolution of the normalized diameter of gyration D_{g_n} for the cases presented in Fig. 11. The growth behavior for the completely stable case with $\mathrm{Pe}=10^3$ and $A=0.762$ is mainly due to the significant diffusion. The strong diffusive effects also explain the larger diameters for $\mathrm{Pe}=10^3$ and $A=0.762$ as compared to the moderate fingering situations of $\mathrm{Pe}=4.0\times10^3$, $A=0.762$ for $\delta=0$, and $\mathrm{Pe}=1.2\times10^4$, $A=0.905$ for $\delta=-5.0\times10^{-6}$ at earlier time periods. For situations showing evident fingering, larger diameters of gyration are observed for higher Péclet numbers, higher viscosity contrast, or weaker Korteweg stresses. Again, stabilizing effects induced by the shrinking droplet area make the curves decay at later times, and strong dispersion induced by small droplets consequently results in underestimated values for D_{g_n}. With the exception of the strongest Korteweg stresses $\delta=-5.0\times10^{-6}$, a more significant increment of gyration diameters always occurs for higher viscosity contrast $A=0.905$. This last finding is in contrast with the behavior displayed in Fig. 11, in which a more significant interfacial length occurs at a higher Péclet number ($\mathrm{Pe}=1.2\times10^4$). These two opposing behaviors can be easily verified by comparing the particular cases for $\mathrm{Pe}=1.2\times10^4$, $A=0.762(\delta=0)$, and $\mathrm{Pe}=4.0\times10^3$, $A=0.905(\delta=0)$ in Figs. 11 and 14. As shown in Fig. 11, while a longer interfacial length is obtained when $\mathrm{Pe}=1.2\times10^4$, $A=0.762$, its diameter of gyration (see Fig. 14) is smaller. This confirms quantitatively the different fingering enhancement mechanisms discussed in Sec. III A, in which more significant finger penetration or competition is caused by a large viscosity contrast, while a high Péclet number mainly leads to branching around a nearly circular region.

IV. CONCLUSION

In this work, we have presented highly accurate numerical simulations for miscible displacement in a time-dependent gap Hele-Shaw cell. The interfacial instabilities have been

analyzed systematically both qualitatively and quantitatively. Our analysis explicitly indicates how the relevant parameters of the system, namely, the Péclet number Pe, the viscosity contrast A, and the surface-tension-like Korteweg stress δ influence the morphology of the interfacial patterns.

First, we studied the situation in which Korteweg stresses were absent ($\delta=0$). In line with the conventional miscible Saffman-Taylor problem with constant gap spacing, we find that more vigorous fingering is observed at higher Péclet number Pe and larger viscosity contrast A. In addition, we have been able to identify the specific roles played by Pe and A in determining different interfacial behaviors. On one hand, we have found that higher Pe's tend to trigger branching on a nearly circular region, leading to longer interfacial lengths. On the other hand, significant finger competition and finger penetration are caused by larger values of A, a morphological feature that can be quantitatively verified by the calculation of larger values of diameter of gyration.

We have also found that the introduction of Korteweg stresses significantly affects the behavior of the mixing interface, introducing important stabilizing effects. In addition, we have verified that if Korteweg stresses are taken into account in a miscible case, the resulting patterns present great resemblance with the structures obtained in the corresponding immiscible situation. Moreover, smooth diffusive effects for the flow with large Pe and A, and with small δ lead to the formation of visually striking interfacial patterns in which the outward fingers pinch off, producing a number of detached droplets. The latter is not explicitly reported in equivalent immiscible flows. Finally, we have shown that such droplet detachment process can be prevented by the action of stronger interfacial stresses. The consistent effects of Korteweg stresses on a miscible interface, and of surface tension on immiscible fluids provide an important and strong evidence that the Korteweg stresses can be treated as an effective interfacial tension in systems including diffusing fluids.

An interesting extension of the current work is the investigation of the influence of magnetic forces on the morphological properties of miscible interfaces in time-dependent gap Hele-Shaw cells. This can be done by assuming that one of the confined fluids is a magnetic fluid (ferrofluid) [58], and a magnetic field is applied. It is well known that, depending on the symmetry properties of the applied magnetic field (perpendicular [21,22], azimuthal [59,60], and radial [43]) it can either stabilize or destabilize the interface. In this sense, an external magnetic field could be used to increase or decrease the miscibility between the fluids [27]. Of course, it would be of interest to investigate how the magnetic field couples to parameters like Pe, A, and δ leading to nontrivial nonlinear behaviors and even more complex interfacial morphologies in miscible magnetic fluids. We plan to perform a detailed study of the latter in a forthcoming paper [61].

ACKNOWLEDGMENTS

J.A.M. thanks CNPq (Brazilian Research Council) for financial support of this research through the CNPq/FAPESQ Pronex program. C.-Y.C. is supported by the National Science Council of the Republic of China under Grant No. NSC 93-2212-E-224-006.

[1] P. G. Saffman and G. I. Taylor, Proc. R. Soc. London, Ser. A **245**, 312 (1958).
[2] D. Bensimon, L. P. Kadanoff, S. Liang, B. I. Shraiman, and C. Tang, Rev. Mod. Phys. **58**, 977 (1986);G. M. Homsy, Annu. Rev. Fluid Mech. **19**, 271 (1987);K. V. McCloud and J. V. Maher, Phys. Rep. **260**, 139 (1995).
[3] L. Paterson, J. Fluid Mech. **113**, 513 (1981).
[4] H. Thomé, M. Rabaud, V. Hakim, and Y. Couder, Phys. Fluids A **1**, 224 (1989).
[5] M. Ben Amar, Phys. Rev. A **44**, 3673 (1991).
[6] Y. Tu, Phys. Rev. A **44**, 1203 (1991).
[7] M. Ben Amar, V. Hakim, M. Mashaal, and Y. Couder, Phys. Fluids A **3**, 1687 (1991).
[8] E. Lajeunesse and Y. Couder, J. Fluid Mech. **419**, 125 (2000).
[9] J. A. Miranda, F. Parisio, F. Moraes, and M. Widom, Phys. Rev. E **63**, 016311 (2001).
[10] F. Parisio, F. Moraes, J. A. Miranda, and M. Widom, Phys. Rev. E **63**, 036307 (2001).
[11] J. A. Miranda, Phys. Rev. E **65**, 026303 (2002).
[12] J. A. Miranda, Phys. Rev. E **65**, 036310 (2002).
[13] J. A. Miranda and F. Moraes, J. Phys. A **36**, 863 (2003).
[14] L. W. Schwartz, Phys. Fluids A **1**, 167 (1989).
[15] Ll. Carrillo, F. X. Magdaleno, J. Casademunt, and J. Ortín, Phys. Rev. E **54**, 6260 (1996).
[16] E. Alvarez-Lacalle, J. Ortín, and J. Casademunt, Phys. Fluids **16**, 908 (2004).
[17] A. Buka, P. Palffy-Muhoray, and Z. Racz, Phys. Rev. A **36**, 3984 (1987).
[18] L. Kondic, M. J. Shelley, and P. Palffy-Muhoray, Phys. Rev. Lett. **80**, 1433 (1998).
[19] M. Constantin, M. Widom, and J. A. Miranda, Phys. Rev. E **67**, 026313 (2003).
[20] P. Fast and M. J. Shelley, J. Comput. Phys. **195**, 117 (2004).
[21] A. O. Tsebers and M. M. Maiorov, Magnetohydrodynamics (N.Y.) **16**, 21 (1980).
[22] D. P. Jackson, R. E. Goldstein, and A. O. Cebers, Phys. Rev. E **50**, 298 (1994).
[23] C. T. Tan and G. M. Homsy, Phys. Fluids **31**, 1330 (1988).
[24] C.-Y. Chen and E. Meiburg, J. Fluid Mech. **371**, 233 (1998); **371**, 269 (1998).
[25] C.-Y. Chen, L. L. Wang, and E. Meiburg, Phys. Fluids **13**, 2447 (2001).
[26] C.-Y. Chen and S. W. Wang, Fluid Dyn. Res. **30**, 315 (2002).
[27] C.-Y. Chen, Phys. Fluids **15**, 1086 (2003).
[28] M. Ruith and E. Meiburg, J. Fluid Mech. **420**, 225 (2000).
[29] E. Meiburg and C.-Y. Chen, SPEJ **5**, 2 (2000).
[30] E. Ben-Jacob, R. Godbey, N. D. Goldenfeld, J. Koplik, H. Levine, T. Mueller, and L. M. Sander, Phys. Rev. Lett. **55**,

1315 (1985).
[31] A. A. Sonin and R. Bartolino, Nuovo Cimento Soc. Ital. Fis., D **15**, 1 (1993).
[32] S.-Z. Zhang, E. Louis, O. Pla, and F. Guinea, Eur. Phys. J. B **1**, 123 (1998).
[33] M. J. Shelley, F-R. Tian, and K. Wlodarski, Nonlinearity **10**, 1471 (1997).
[34] S. Sinha, S. K. Kabiraj, T. Dutta, and S. Tarafdar, Eur. Phys. J. B **36**, 297 (2003).
[35] S. K. Kabiraj and S. Tarafdar, Physica A **328**, 305 (2003).
[36] J. A. Miranda and R. M. Oliveira, Phys. Rev. E **69**, 066312 (2004).
[37] B. A. Francis and R. G. Horn, J. Appl. Phys. **89**, 4167 (2001).
[38] D. Derks, A. Lindner, C. Creton, and D. Bonn, J. Appl. Phys. **93**, 1557 (2003).
[39] S. Poivet, F. Nallet, C. Gay, and P. Fabre, Europhys. Lett. **62**, 244 (2003).
[40] M. Tirumkudulu, W. B. Russel, and T. J. Huang, Phys. Fluids **15**, 1588 (2003).
[41] R. D. Welsh, M.S. thesis, Massachusetts Institute of Technology, 2001.
[42] J. A. Miranda, Phys. Rev. E **69**, 016311 (2004).
[43] J. A. Miranda, R. M. Oliveira, and D. P. Jackson, Phys. Rev. E **70**, 036311 (2004).
[44] D. Korteweg, Arch. Neel. Sci. Ex. Nat. **II**, 6 (1901).
[45] D. Joseph, Eur. J. Mech. B/Fluids **9**, 565 (1990).
[46] G. Galdi, D. Joseph, L. Prezisi, and S. Rionero, Eur. J. Mech. B/Fluids **10**, 565 (1991).
[47] H. Hu and D. Joseph, ZAMP **43**, 626 (1992).
[48] D. Joseph, A. Huang, and H. Hu, Physica D **97**, 104 (1996).
[49] C.-Y. Chen and E. Meiburg, Phys. Fluids **14**, 2052 (2002).
[50] G. I. Taylor, Proc. R. Soc. London, Ser. A **219**, 186 (1953).
[51] P. Petitjeans and T. Maxworthy, J. Fluid Mech. **326**, 37 (1996).
[52] C.-Y. Chen and E. Meiburg, J. Fluid Mech. **326**, 57 (1996).
[53] J. Fernandez, P. Kurowski, L. Limat, and P. Petitjeans, Phys. Fluids **13**, 3120 (2001).
[54] J. Fernandez, P. Kurowski, P. Petitjeans, and E. Meiburg, J. Fluid Mech. **451**, 239 (2002).
[55] F. Graf, E. Meiburg, and C. Hartel, J. Fluid Mech. **451**, 261 (2002).
[56] N. Goyal and E. Meiburg, J. Fluid Mech. **516**, 211 (2004).
[57] J. B. Segur, in *Glycerol*, edited by C. S. Miner and N. N. Dalton (Reinhold, New York, 1953).
[58] R. E. Rosensweig, *Ferrohydrodynamics* (Cambridge University Press, Cambridge, U. K., 1985), and references therein.
[59] J. A. Miranda, Phys. Rev. E **62**, 2985 (2000).
[60] D. P. Jackson and J. A. Miranda, Phys. Rev. E **67**, 017301 (2003).
[61] C.-Y. Chen, C.-H. Chen, and J. A. Miranda (unpublished).